Nonlinear absorption in a series of Donor–π–Acceptor cyanines with different conjugation lengths†

Lazaro A. Padilha,*[a] Scott Webster,[a] Olga V. Przhonska,[ab] Honghua Hu,[a] Davorin Peceli,[a] Jonathan L. Rosch,[a] Mikhail V. Bondar,[b] Andriy O. Gerasov,[c] Yuriy P. Kovtun,[c] Mykola P. Shandura,[c] Alexey D. Kachkovski,[c] David J. Hagan[a] and Eric W. Van Stryland[a]

Received 14th April 2009, Accepted 14th May 2009
First published as an Advance Article on the web 23rd June 2009
DOI: 10.1039/b907344b

A detailed experimental and theoretical study of the linear and nonlinear absorption of a series of asymmetrical D–π–A cyanine dyes with the same trimethylindolin donor (D) and diethylamino-coumarin-dioxaborine acceptor (A) terminal groups and different conjugation lengths, is presented. Strong solvatochromic behavior affecting the fluorescence quantum yields, lifetimes, and the linear and nonlinear absorption properties is observed due to the presence of permanent ground state dipole moments. Detailed experimental studies of lifetime dynamics are performed by direct time-correlated single photon counting and pump–probe techniques. We find that an increase in π-conjugation in the investigated series of dyes leads to an enhancement of the excited-state absorption and two-photon absorption (2PA) cross-sections (δ_{2PA}). The 2PA spectra for all of the investigated dyes consist of two well-separated bands. The first band occurs at two-photon excitation into the vibrational levels and not into the absorption peak of the main transition, $S_0 \rightarrow S_1$, which is more typical of that observed for symmetrical cyanines. The position of the second 2PA band for all the molecules remains unchanged in solvents of different polarity contrary to the large solvatochromic shift of the $S_0 \rightarrow S_1$ band, resulting in a large intermediate state resonance enhancement and, therefore, a larger 2PA in acetronitrile ($\delta_{2PA} \approx 10000$ GM) compared to toluene ($\delta_{2PA} \approx 4700$ GM).

Introduction

Molecular nonlinear optics has attracted considerable attention for the few past decades, mainly due to potential applications in various fields, including telecommunications, optical data storage and optical information processing, optical switching, micro-fabrication, and optical imaging of biological media.[1–4] Significant experimental and theoretical studies have been devoted to designing molecules with optimized nonlinear optical responses and to understanding their structure–property relationships. For many organic structures, including cyanines, delocalized electrons in their π-conjugated systems are known to be the primary source of nonlinearity at the molecular level. Insertion of electron-donor (D) and electron-acceptor (A) groups into the π-conjugated backbone typically leads to increases in the nonlinear properties and allows for a variety of sophisticated molecular designs. These compounds often contain the following structures: D–π–D (*e.g.*, cationic symmetrical polymethines[5]), D–π–A–π–D (*e.g.*, symmetrical polymethine-like squaraines or polyene-like tetraones[6]), A–π–A or A–π–D–π–A (*e.g.*, symmetrical oxaborines or fluorenes[7–9]) and asymmetrical D–π–A molecules, frequently referred to as push–pull polyenes.[10–12] The linear and nonlinear optical properties of asymmetrical compounds can be significantly influenced by the polarity of their environment.[13–16]

In previous studies we have shown that squaraines, with D–π–A–π–D structures, have much stronger two-photon absorption (2PA) than similar polymethines with D–π–D having the same conjugation length.[6,17] Quantum-chemical calculations show that an increase in the density of final states, originating from the squaraine acceptor, enhances the 2PA.[17] Recent publications have shown that extended squaraines can exceed 30,000 GM at the peak 2PA.[18] In the current work we perform a detailed experimental and quantum-chemical investigation of the linear and nonlinear absorption of a new series of asymmetric D–π–A cyanines with different conjugation lengths. We observe 2PA cross-section values for these asymmetrical dyes that are comparable to previously studied symmetrical squaraines.

In the following sections of this paper we will describe: (1) electronic structure of asymmetrical D–π–A molecules along with their linear absorption, fluorescence properties in solvents of different polarities, and lifetime measurements; (2) experimental methods used for determining 2PA and ESA, and their results; (3) a two-state model to explain their linear spectroscopic properties; and (4) the 2PA spectral analysis that provides insights into their nature.

2. Experimental methods and results

2.1. Materials characterization and linear spectroscopic properties

The molecular structures of the dyes studied in this paper are shown in the inset of Fig. 1a–c. Their chemical names are:

[a]*CREOL, The College of Optics and Photonics, University of Central Florida, Orlando, FL, 32826. E-mail: padilha@creol.ucf.edu*
[b]*Institute of Physics, National Academy of Sciences, Kiev, 03028, Ukraine*
[c]*Institute of Organic Chemistry, National Academy of Sciences, Kiev, 03094, Ukraine*

† This paper is part of a *Journal of Materials Chemistry* theme issue on organic non-linear optics. Guest editor: Seth Marder.

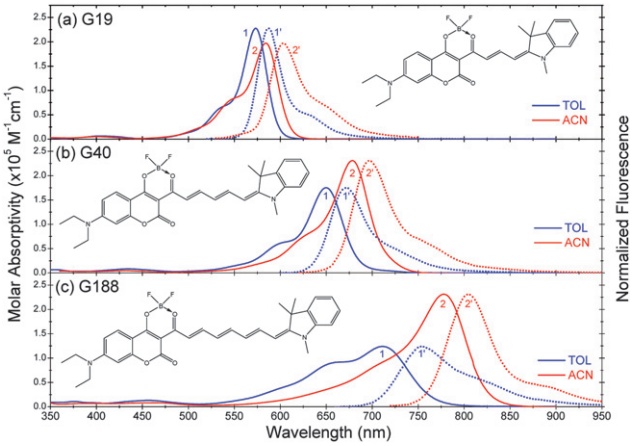

Fig. 1 Molar absorptivities (1 and 2) and normalized fluorescence (1′ and 2′) spectra in toluene and acetonitrile (ACN), respectively, of G19 (a), G40 (b), and G188 (c). Insets contain molecular structures.

8-(diethylamino)-2,2-difluoro-5-oxo-(5H)-4-[3-(1,3,3-trimethylindolin-2-ylidene)-1-propenyl]-chromeno[4,3-d]-1,3,2-(2H)-dioxaborine, labelled as G19; 8-(diethylamino)-2,2-difluoro-5-oxo-(5H)-4-[5-(1,3,3-trimethylindolin-2-ylidene)-1,3-pentadienyl]-chromeno [4,3-d]-1,3,2-(2H)-dioxaborine, labelled as G40, and 8-(diethylamino)-2,2-difluoro-5-oxo-(5H)-4-[7-(1,3,3-trimethylindolin-2-ylidene)- 1,3,5-heptatrienyl]-chromeno[4,3-d]-1,3,2-(2H)-dioxaborine, labelled as G188. All three dyes contain trimethylindolin donor (D) and diethylamino-coumarin-dioxaborine acceptor (A) terminal groups, which themselves possess delocalized π-electron systems and may increase the overall π-conjugation, and different lengths of the vinylene chain; G19 being the shortest with n = 1 and G188 the longest with n = 3.

The synthesis of G19 and G40 was recently described in Ref. 19. The synthesis of G188 was performed by a similar way.‡ The linear absorption spectra of all molecules, recorded by a Varian Cary 500 spectrophotometer, are presented in Fig. 1a–c with the most significant linear properties listed in Table 1. Most measurements were performed in two solvents with different polarity, spectroscopic grade toluene and acetonitrile (ACN). It is known that the polarity of solvents can be characterized by their orientational polarizability, which is given by $\Delta f = (\varepsilon - 1)/(2\varepsilon + 1) - (n^2 - 1)/(2n^2 + 1)$, where ε is the static dielectric constant and n is the refractive index of the solvent.[20] Calculated Δf values are: 0.013 for toluene and 0.306 for ACN. The absorption spectra for all dyes are composed of intense cyanine-like bands, attributed to the $S_0 \rightarrow S_1$ absorption, with the main absorption peaks shifted by ≈100 nm to longer wavelengths with lengthening of the main conjugation chain, and weak linear absorption in the visible and UV region corresponding to absorption to higher excited states $S_0 \rightarrow S_n$. Increasing solvent polarity from toluene to ACN leads to a bathochromic shift of the main absorption peak, ≈11 nm for G19, ≈28 nm for G40, and ≈65 nm for G188. This large shift in absorption demonstrates their strong polar solvatochromic behavior, which is well-known for merocyanine dyes with a large ground-state permanent dipole moment.[21] The solvatochromic behavior of such molecules in solution can be explained by the comparison of their permanent dipole moments in the ground (μ_0) and excited states (μ_1). If the excited state exhibits a larger dipole moment than the ground state, $\mu_1 > \mu_0$, it is preferentially stabilized by the more polar solvent, and the energy between these two states decreases, that is, the absorption and emission spectra both shift to the red region as seen in Fig. 1a–c. Additionally, note that the less polar solvent, toluene, leads to a substantial band broadening for G188 evidenced by the increase in the shoulder of the main transition. A more detailed analysis of the effect of solvent polarity is discussed in Section 3.

The fluorescence spectra of all compounds in toluene and ACN, measured by a PTI QuantaMaster spectrofluorimeter equipped with a nitrogen cooled (77 K) Hamamatsu R5509-73 photomultiplier, are also shown in Fig. 1a–c. All fluorescence spectra are corrected for the spectral responsivity of the photomultiplier. Fluorescence quantum yields, η, are measured using the standard method of comparison for G19 and G40 with a known "red" standard dye, Cresyl Violet perchlorate (CAS# 41830-80-2, Sigma Aldrich) in methanol, which has an absorption peak at 594 nm, fluorescence peak at 620 nm, and a fluorescence quantum yield, η, of 0.54.[22] The fluorescence quantum yield for G188 was measured by comparison with our previously proposed standard for the near infrared wavelength range, dye PD 2631 in ethanol, with an absorption peak at 784 nm, fluorescence peak at 809 nm and $\eta = 0.11 \pm 0.01$.[23] Results of the quantum yield measurements are listed in Table 1. As shown, polarity of the solvent significantly affects not only the positions of absorption and fluorescence spectra but also the fluorescence quantum yields. The largest difference in quantum yield is observed for G19 (8 times larger in toluene). In order to investigate the effect of solvent polarity in more detail, we performed quantum yield and lifetime measurements in mixtures of toluene and ACN, which allows us to continuously change solvent polarity in the range 0.013–0.306. Polarity dependent quantum yield and lifetime measurements are presented in Fig. 2a–b. The peak absorption of G19 in Fig. 1a shows a slight reversal trend in its position (~2 nm) at polarities larger than $\Delta f \sim 0.26$. This reproducible result was meticulously studied by the following procedures: (1) premixing toluene and ACN followed by the addition of G19; (2) dissolving G19 in toluene followed by the appropriate dilution of ACN; and (3) dissolving G19 in ACN followed by the appropriate dilution of toluene. All dye concentrations in toluene-ACN mixtures were kept similar, confirmed by measuring the absorbance and maintaining a constant optical density (1.0 ± 0.1). Although we do not understand the nature of this shift, we presume it is related to a change of the ground state electronic structure, from $\mu_1 > \mu_0$ to $\mu_0 > \mu_1$.

It is seen that the fluorescence quantum yield and lifetime of G19 gradually decreases with increasing solvent polarity. For example, the combination of 20% ACN by volume into toluene leads to their decrease by a factor of two. From spectroscopic

‡ M.p. 250–1 °C. ^{1}H NMR ($CDCl_3$) δ: 1.18 (t, $^3J_{H,H} = 6.9$ Hz, 6 H), 1.56 (s, 6 H), 3.21 (s, 3 H), 3.40 (q, $^3J_{H,H} = 6.9$ Hz, 4 H), 5.55 (d, $^3J_{H,H} = 12.2$ Hz, 1 H), 6.21 (m, 1 H), 6.29 (s, 1 H), 6.44 (m, 1 H), 6.55 (d, $^3J_{H,H} = 9.3$ Hz, 1 H), 6.73 (d, $^3J_{H,H} = 7.0$ Hz, 1 H), 6.94 (m, 1 H), 7.06 (m, 1 H), 7.18 (m, 2 H), 7.27 (m, 1 H), 7.62 (d, $^3J_{H,H} = 13.9$ Hz, 1 H), 7.86 (d, $^3J_{H,H} = 9.3$ Hz, 1 H), 8.06 (m, 1 H). Anal. calcd. for $C_{32}H_{33}BF_2N_2O_4$: C, 68.83; H, 5.96; N, 5.02. Found: C, 68.72; H, 5.92; N, 5.04

Table 1 Spectroscopic parameters of G19, G40, and G188 in toluene and acetonitrile (ACN): λ^{max}_{Abs} and λ^{max}_{Fl} are the peak absorption and fluorescence wavelengths; ε^{max} are the peak extinction coefficients; η and τ_F are the fluorescence quantum yields and lifetimes; and μ_{01} are the transition dipole moments, respectively

Dye (Solvent)	λ^{max}_{Abs} (nm)	λ^{max}_{Fl} (nm)	ε^{max} ($\times 10^{-5}$ M^{-1} cm^{-1})	η	τ_F Calculated from Eq. 1(ns)	τ_F Time resolved Fluorescence (ns)	τ_F Picosecond Pump–Probe	μ_{01} Transition Dipole Moment (Debye)
G19 (toluene)	572	587	2.28	1.0 ± 0.1	2.0 ± 0.4	1.9 ± 0.4	—	12.6
G19 (ACN)	583	603	1.95	0.12 ± 0.01	0.3 ± 0.1	0.5 ± 0.2	—	13.1
G40 (toluene)	650	672	1.75	0.81 ± 0.08	2.3 ± 0.5	1.9 ± 0.4	1.7 ± 0.3	13.1
G40 (ACN)	678	698	2.31	0.52 ± 0.05	1.6 ± 0.3	1.5 ± 0.5	1.5 ± 0.3	15
G188 (toluene)	712	754	1.24	0.34 ± 0.03	1.2 ± 0.2	1.1 ± 0.2	1.0 ± 0.2	14.7
G188 (ACN)	777	805	2.32	0.19 ± 0.02	0.7 ± 0.3	1.1 ± 0.2	1.0 ± 0.2	17.1

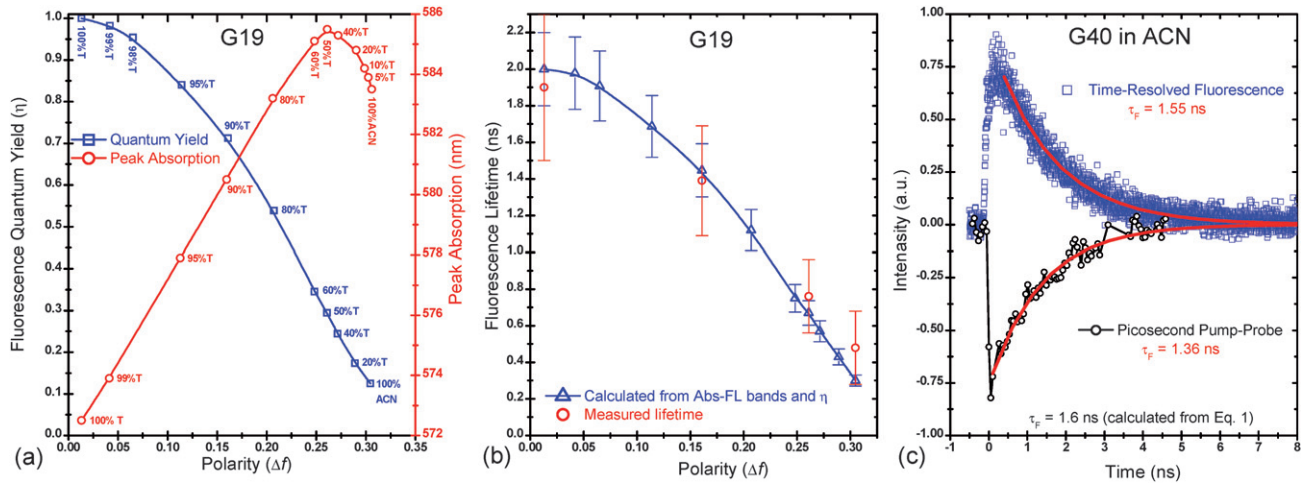

Fig. 2 (a) Fluorescence quantum yield (blue squares) and peak ground-state absorption wavelength (red circles) as a function of solvent polarity for G19. Note: a reversal trend in peak absorption positions starting at 60% ACN and 40% toluene mixtures, presumably connected with a dominant specific interaction between the dye molecule and polar solvent shell. (b) Comparison of fluorescence lifetime (blue triangles), calculated from Eqn 1, and measured by time-resolved fluorescence (red circles) as function of solvent polarity for G19. (c) Time-resolved fluorescence (blue squares) and picosecond pump–probe measured at 532 nm (black circles) for G40 in ACN.

measurements, we estimated the fluorescence lifetime $\tau_F = \eta\tau_R$, where the natural lifetime τ_R can be calculated from:[20]

$$1/\tau_R = 2.88 \times 10^{-9} n^2 \varepsilon^{max} \left[\frac{\int F(\nu)\mathrm{d}\nu \times \int \frac{\varepsilon(\nu)}{\nu}\mathrm{d}\nu}{\int \frac{F(\nu)}{\nu^3}\mathrm{d}\nu} \right] \quad (1)$$

where $F(\nu)$and $\varepsilon(\nu)$ are the normalized fluorescence and absorption spectra, and ε^{max} is the extinction coefficient at the peak absorption. Calculated fluorescence lifetimes are the following: 0.30 ± 0.05 ns in ACN and 2.0 ± 0.1 ns in toluene for G19; 1.60 ± 0.05 ns in ACN and 2.3 ± 0.1 ns in toluene for G40, and 0.70 ± 0.05 ns in ACN and 1.2 ± 0.1 ns in toluene for G188.

For many cyanine-like molecules with spectral mirror symmetry between absorption and fluorescence spectra, and small changes in excited state geometry, Eqn (1) gives reasonably good agreement with the measured lifetime values.[23] However, for asymmetrical donor–acceptor molecules with permanent ground and excited-state dipole moments showing solvatochromic behavior, these lifetimes must be experimentally verified. Therefore, τ_F was measured directly by a time-correlated single photon counting system (PicoQuant, PicoHarp300) collecting the complete fluorescence spectrum with an instrument response time of ~200 ps. The samples were pumped by linearly polarized, 100 fs (FWHM) laser pulses at a wavelength of 390 nm from a frequency doubled Ti:sapphire femtosecond laser (Coherent Inc., Mira). The excitation polarization was oriented at the magic angle (54.7°) with respect to the detected emission polarization. Measurements were performed for G19, G40, and G188 in toluene and ACN. For G19, additional solutions were measured in toluene-ACN mixtures (90% toluene-10% ACN corresponding to 0.16 polarity and 50% toluene-50% ACN, corresponding to 0.26 polarity). Results for G19 in different solvents are presented in Fig. 2b. It is seen that an increase in solvent polarity leads to a strong decrease in the fluorescence quantum yield and lifetimes. Based on these results, we can conclude that G19 is very sensitive to solvent polarity and can be used as an efficient probe to test the polarity of microenvironments. The largest discrepancy between measured and calculated values is observed for the shortest lifetime (in pure ACN). However, in this case the fluorescence signal is very weak and the response time of our equipment is comparable to the calculated lifetime. In general, experimental results for all dyes agree to within 30% of the values calculated from the fluorescence quantum yield (see Table 1).

For additional verification of the fluorescence lifetimes, picosecond degenerate pump–probe measurements at 532 nm (as

described in detail in Ref. 6), were performed for G40 and G188. No measurable signal was obtained for G19 at 532 nm presumably due to the equal ground and excited-state absorption cross-sections. Fig. 2c shows a comparison of lifetime data obtained from both methods for G40 in ACN. As seen, both methods agree reasonably well with each other.

The spectral positions of the optical transitions and the orientation of the transition dipole moments can be determined by one-photon excitation anisotropy measurements.[20] These measurements are performed using a PTI QuantaMaster Spectrofluorimeter using viscous solutions to reduce rotational reorientation and at low concentrations ($C \approx 10^{-6}$ M) to avoid reabsorption of the fluorescence. The anisotropy, calculated by $r(\lambda) = \frac{I_{II}(\lambda) - I_{\perp}(\lambda)}{I_{II}(\lambda) + 2I_{\perp}(\lambda)}$, is measured by observing the emission wavelength, typically near the fluorescence maximum, with a fixed polarization. Then, the fluorescence intensity is recorded as a function of excitation wavelength λ at polarizations parallel ($I_{II}(\lambda)$) and perpendicular ($I_{\perp}(\lambda)$) to the emission polarization. Emission anisotropy, which can give information about molecular vibrational depolarization, was measured and calculated in the same way; the only difference is that these measurements are performed by fixing an excitation wavelength and tuning the emission wavelength through the fluorescence. Experimentally, no depolarization is observed within the entire emission range for all the dyes. Shown in Fig. 3 are the absorption, fluorescence and anisotropy spectra in polytetrahydrofuran (pTHF) of average

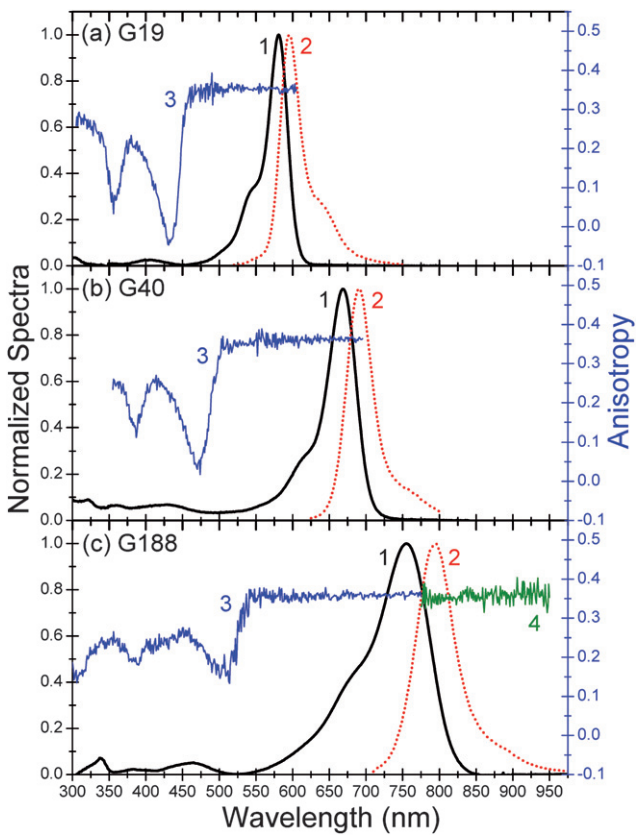

Fig. 3 Absorption (1), fluorescence (2) and excitation anisotropy (3) spectra of G19 (a), G40 (b), and G188 (c) in pTHF. Emission anisotropy (4) spectrum for G188 (c) in pTHF.

$M_n \sim 1000$ (CAS# 25190-06-1). We observe that the excitation anisotropy spectra reveal the large alternation of peak and valley features for all molecules, in spite of their asymmetrical structure, which is quite an unusual result. This alternation indicates that the molecules can be characterized by one-photon allowed and symmetry-forbidden transitions similar to symmetrical dyes. It is worth noting that this information cannot be obtained from the linear absorption spectra alone. Analysis of the anisotropy spectra, linked to quantum-chemical calculations, allows us to estimate the angles between electron transitions and find the positions of one-photon forbidden transitions, *i.e.* transitions between states of the same symmetry, and therefore, possible positions of 2PA bands. As shown in Fig. 3, the excitation anisotropy function $r(\lambda)$ is constant ($r \approx 0.35$) in the broad spectral range 450–600 nm for G19, 500–700 nm for G40, and 600–850 nm for G188, indicating a nearly parallel orientation of the absorption (within the band $S_0 \rightarrow S_1$) and the emission $S_1 \rightarrow S_0$ transition dipole moments. In the shorter wavelength region, the anisotropy spectra show two minima at ≈430 nm and ≈350 nm for G19, at ≈470 nm and ≈380 nm for G40, and three minima at ≈510 nm, 380 nm and ≈305 nm for G188, corresponding to one-photon forbidden transitions $S_0 \rightarrow S_n$ forming 40–60° angles with the emission dipole moment. Based on quantum-chemical calculations, we conclude that the first minimum in the excitation anisotropy spectra (430 nm, 470 nm and 580 nm) correspond to the transition $S_0 \rightarrow S_2$ in the linear absorption and indicate the possible positions of the final states in 2PA spectra for these dyes. Values for the transition dipole moments $\boldsymbol{\mu}_{01}$ for all molecules are calculated from the integrated main absorption band $S_0 \rightarrow S_1$: $\mu_{01} = \{[1500(\hbar c)^2 \ln 10] \int \varepsilon_{01}(\nu) d\nu / \pi N_A E_{01}\}^{1/2}$, where $\varepsilon_{01}(\nu)$ is the extinction coefficient, N_A is Avogadro's number, and E_{01} is the peak energy.[20] Calculations indicate that all dyes have similar μ_{01} values from 13 to 17 D, being slightly larger in ACN than in toluene as shown in Table 1.

2.2. Nonlinear characterization methods and results

The nonlinear optical characterization for the series of asymmetric cyanines is performed using laser systems with femtosecond (for 2PA and ESA spectra) and picosecond (for ESA dynamics) pulsewidths. The femtosecond system consists of a Clark-MXR Ti:Sapphire regenerative amplifier, CPA-2010, delivering 2 mJ pulses at 775 nm and 140 fs (FWHM) pulsewidth at a 1 kHz repetition rate. The CPA-2010 pumps two optical parametric generator/amplifiers (OPG/OPA Light Conversion Ltd., model TOPAS-800); both TOPAS can be tuned independently from 300 nm to 2.6 μm with pulsewidths 100–140 fs (FWHM). The picosecond system consists of a 10 Hz modelocked Nd:YAG laser (EKSPLA, model PL2143) operating at 1064 nm and is frequency tripled to pump an OPG/OPA (EKSPLA, model PG401 DFG) tunable from 420 nm to 18 μm with a pulsewidth in the visible of 15 ps (FWHM), measured by second harmonic autocorrelation.

The ESA spectra are measured using the femtosecond pump and white-light continuum (WLC) probe as described in Ref. 24. Two OPG/OPA systems are used, one of them, used as the pump, is set at the wavelength of the peak linear absorption of each investigated sample, while the second OPG/OPA is set at 1300 nm and weakly (~10 μJ) pumps a CaF_2 crystal to generate a weak

but stable and broadband WLC, which is used as a probe. In order to improve the signal to noise ratio and avoid stimulated emission,[25] instead of using the complete WLC spectrum all at once, narrow band spectral filters (~10 nm) are used to select the probe wavelengths. Several filters with different central wavelengths are used to obtain the complete ESA spectrum. The probe spot size at the sample is ~10× smaller than the pump and the angle between pump and probe is small, ~5°, to assure that the probe travels through the homogeneously pumped solution. The fluence of the probe is kept below 5% of the pump to avoid nonlinearities from the probe. For each probe wavelength λ, the ESA cross-section, $\sigma_{1n}(\lambda)$, is calculated by Eqn (2):

$$T_L(\lambda) = \exp\left[-\sigma_{01}(\lambda)NL\right]$$
$$T_{NL}(\lambda) = \exp\left[-\sigma_{01}(\lambda)N_0L - \sigma_{1n}(\lambda)N_1L\right] \quad (2)$$

where $T_L(\lambda)$ is the linear transmittance measured by a Cary 500 spectrophotometer; $T_{NL}(\lambda)$ is the transmittance of the probe beam in the presence of the pump with a delay of ~1 ps; L is the sample thickness (1 mm cell); N is the number of molecules per unit volume, calculated from the sample concentration, while N_0 and N_1 are the corresponding number of molecules in the ground and the first excited states: $N = N_0 + N_1$. We assume that the number of molecules in the higher excited states is negligible due to its very fast relaxation time. The ground-state cross-section, $\sigma_{01}(\lambda)$, is also known from linear absorption measurements.

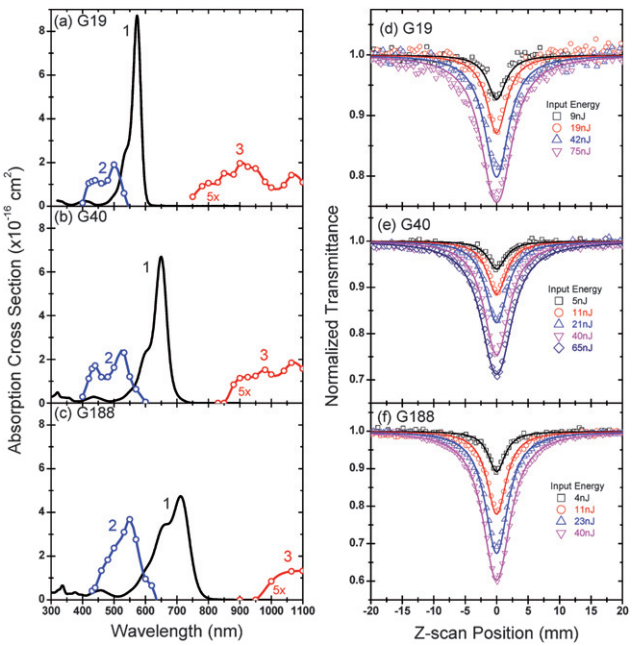

Fig. 4 One-photon (1) and excited-state absorption spectra in the visible (2) and near infrared (3) for G19 (a), G40 (b), and G188 (c) in toluene. Note: NIR spectra in Fig. (a–c) have been multiplied by five for clarity. Open-aperture picosecond Z-scan measurements using (d) 8 ps FWHM at 500 nm for G19, and (e) 11 ps FWHM at 532 nm for G40 and (f) G188 in toluene. The fittings are done using a 3-level model with the following set of parameters: (d) $\sigma_{01} = 5 \times 10^{-17}$ cm^2, $\sigma_{1n} = 19 \times 10^{-17}$ cm^2, $\tau_{10} = 1.9$ ns, $\tau_{21} = 1$ ps, (e) $\sigma_{01} = 3.1 \times 10^{-17}$ cm^2, $\sigma_{1n} = 23 \times 10^{-17}$ cm^2, $\tau_{10} = 1.9$ ns, $\tau_{21} = 2.5$ ps, (f) $\sigma_{01} = 2.3 \times 10^{-17}$ cm^2, $\sigma_{1n} = 31 \times 10^{-17}$ cm^2, $\tau_{10} = 1.1$ ns, $\tau_{21} = 4.5$ ps.

Fig. 4 shows the ESA spectra measured for samples G19, G40, and G188 in toluene. The absolute values for $\sigma_{1n}(\lambda)$ and N_1 are obtained using the values of $\sigma_{1n}(\lambda_{ESA})$, measured independently by picosecond Z-scans[26] at different wavelengths, λ_{ESA}, typically close to the ESA peak for each molecule, using Eqn (3):[27]

$$\sigma_{1n}(\lambda) = \sigma_{01}(\lambda) - \left(\sigma_{01}(\lambda_{ESA}) - \sigma_{1n}(\lambda_{ESA})\right) \times \frac{\ln\left(T_{NL}/T_L\big|_{\lambda}\right)}{\ln\left(T_{NL}/T_L\big|_{\lambda_{ESA}}\right)} \quad (3)$$

The picosecond Z-scan setup alignment and focused beam spot size was verified at every wavelength by measuring the nonlinear refractive index of neat carbon disulfide (CS_2) *via* closed aperture Z-scan.[26] The measurements were performed at 500 nm for G19, and 532 nm for G40 and G188. For each sample, Z-scan measurements were performed at several input energies and were fit based on a three level model, using the rate and propagation equations:

$$\frac{dI}{dz} = -\sigma_{01}N_0I - \sigma_{1n}N_1I$$
$$\frac{dN_0}{dt} = -\frac{\sigma_{01}N_0I}{\hbar\omega} + \frac{N_1}{\tau_F}$$
$$\frac{dN_1}{dt} = \frac{\sigma_{01}N_0I}{\hbar\omega} - \frac{N_1}{\tau_F} - \frac{\sigma_{1n}N_1I}{\hbar\omega} + \frac{N_2}{\tau_{21}} \quad (4)$$
$$\frac{dN_2}{dt} = \frac{\sigma_{1n}N_1I}{\hbar\omega} - \frac{N_2}{\tau_{21}}$$

where $N = N_0 + N_1 + N_2$, and τ_{21} is the nonradiative decay from the state S_2.

The picosecond Z-scan results and fits are shown in Fig. 4(d–f). The fitting is performed using Eqn (4) and the experimentally measured values for τ_F. The only free parameters used for the fittings are τ_{21} and σ_{1n}. For each sample the fitting for all energies is done using the same set of parameters. From these results it is found that the maximum ESA cross-section and wavelength are $\sigma_{1n}(500\text{ nm}) = 1.9 \times 10^{-16}$ cm^2 for G19, $\sigma_{1n}(525\text{ nm}) = 2.4 \times 10^{-16}$ cm^2 for G40, and $\sigma_{1n}(550\text{ nm}) = 3.7 \times 10^{-16}$ cm^2 for G188. The error bars are ~ ±15% for the ESA maximum values. Further discussion of ESA is found in Sec. 3.1.

The degenerate 2PA spectrum is measured in all three samples in toluene and ACN. The 2PA characterization is performed by two experimental methods, two-photon excited fluorescence (2PF) and single wavelength femtosecond open aperture Z-scan. The 2PF technique is more sensitive for measuring samples with relatively high fluorescence quantum yield (>1%), and it is used specially to measure the weak 2PA band close to the 2PA edge (at excitation wavelengths far from the linear absorption). The 2PF experiment is performed using the tunable femtosecond source as described in Ref. 28. For each wavelength measured, the 2PA cross-section is calculated based on known reference samples Rhodamine B in methanol,[28] and the quadratic dependence of the fluorescence on the pump irradiance is also verified to avoid any possible influence of one-photon excited fluorescence (1PF) on the results. Close to the linear absorption edge scattered pump

and/or 1PF can lead to inaccurate and erroneous results, so the results have to be double-checked by open aperture Z-scan. However, linear absorption can lead to excited-state absorption which can be indistinguishable from the 2PA in the open aperture Z-scan measurement without additional measurements. To assure the absence of ESA contributions to the 2PA spectrum, femtosecond pump–probe is used to investigate the response time of the nonlinearity.[6]

For sample G188, a significant portion of the fluorescence spectrum is longer than 800 nm and is beyond the calibrated detection limit of our 2PF system, so it was not possible to obtain the absolute values of the 2PA cross-section *via* 2PF. For this case, only the shape of the spectrum was obtained by 2PF and open aperture Z-scan was performed to measure the absolute value of the cross-sections. For every wavelength, the femtosecond Z-scan is aligned and calibrated by measuring the 2PA and nonlinear refractive index of semiconductors, ZnSe (for $\lambda < 900$ nm) and CdTe (for $\lambda > 900$ nm), and the nonlinear refractive index of CS_2. The 2PA spectra for G19, G40, and G188 in both solvents are shown in Fig. 5, Fig. 6 and Fig. 7 respectively, and discussed in Sec. 3.2. Examining the 2PA spectra from both 2PF and Z-scan measurements, excellent agreement in 2PA magnitude is observed for G19 and G40, as well as the shape of the strong 2PA band for G188 indicating that scaling of 2PF by Z-scan is reasonable and accurate.

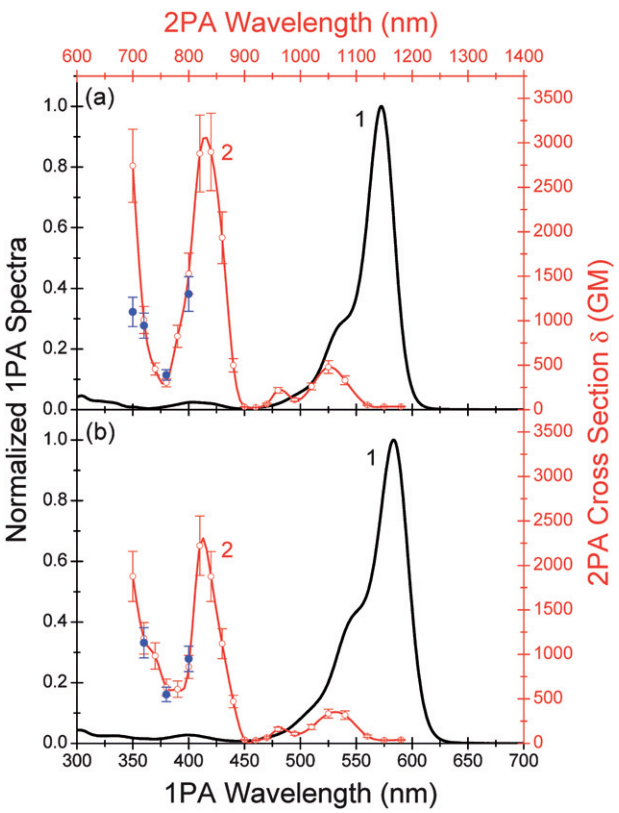

Fig. 5 Normalized one-photon (1) and two-photon absorption spectra (2) for G19 in toluene (a) and acetonitrile (b). Two-photon absorption spectra were obtained by two-photon fluorescence (red circles) and by single wavelength Z-scan (blue solid circles).

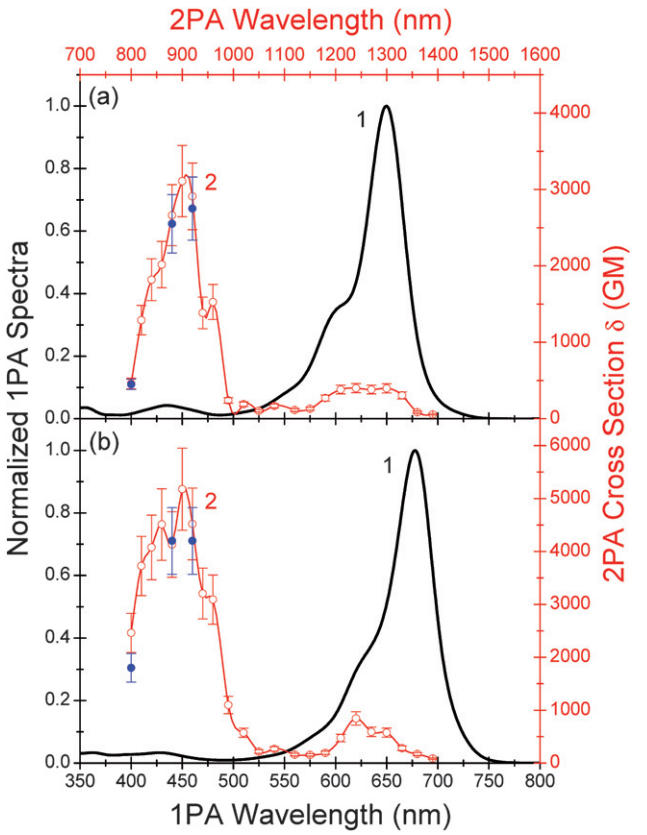

Fig. 6 Normalized one-photon (1) and two-photon absorption spectra (2) for G40 in toluene (a) and acetonitrile (b). Two-photon absorption spectra were obtained by two-photon fluorescence (red circles) and by single wavelength Z-scan (blue solid circles).

3. Discussion

3.1. Two-state model for explanation of linear spectroscopic properties

The main properties of the compounds can be explained based on the well-developed two-state model for push-pull polyenes as quasi-one-dimensional molecules containing an electron-donating group D and electron-accepting group A interacting *via* a π-conjugated chromophore.[29,30] The structure of these molecules can be presented in two resonance forms: neutral (D–π–A) and ionic (or zwitterionic) with the separated charges (D^+–π–A^-). Using this model in conjunction with extensive experimental data and quantum-chemical analysis, valuable insights may be gained for the explanation of the linear and nonlinear properties of G19, G40 and G188. Our understanding is that for the molecule G19 with the shortest conjugated chain, the donor–acceptor properties of the terminal groups in both solvents dominate over the properties of the polyenic chain, and the ground state can be represented by a "polymethine-like" structure with almost equalized bond lengths within the conjugated chromophore and with the charges alternating at carbon atoms. This is confirmed by very similar shapes of the absorption bands in ACN and toluene (Fig. 1a) and X-ray crystallography measurements, which were performed in monocrystals at 293 K on a Bruker Smart Apex II Diffractometer. The molecular geometry for the single orthorhombic crystal of G19 was determined from X-ray

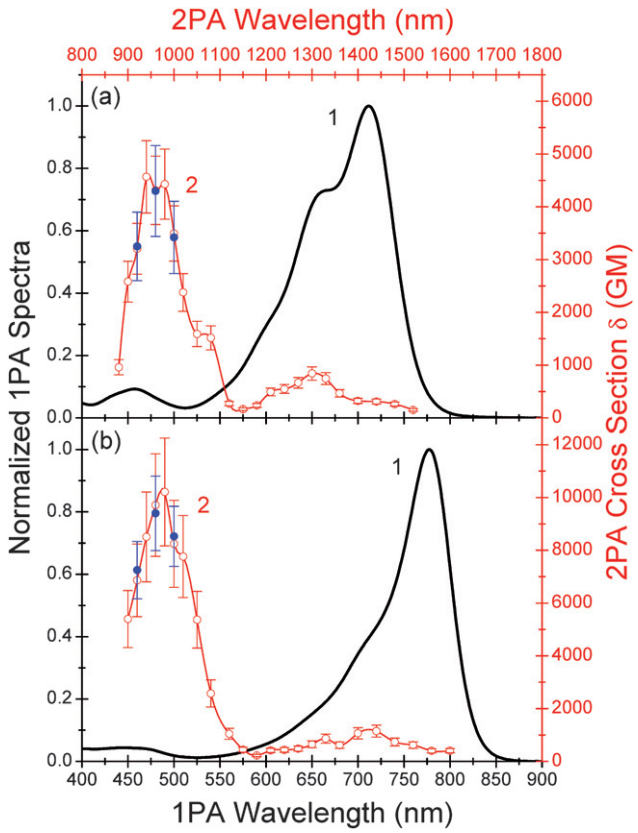

Fig. 7 Normalized one-photon (1) and two-photon absorption spectra (2) for G188 in toluene (a) and acetonitrile (b). Two-photon absorption spectral shapes were obtained by two-photon fluorescence (red circles) and scaled by single wavelength Z-scan (blue solid circles).

diffraction data using the CRYSTALS program package[31] and is presented in Fig. 8. Bond length alternation (BLA) within the chain from C1 to C14 is larger than is typical for symmetrical polymethine dyes. However, the bond length differences are much smaller than for the typical polyenic structure ($\approx$0.1 Å),[32,33] which is determined by the properties of the terminal groups. As a result of electron transition $S_0 \rightarrow S_1$, charge is transferred to the neighboring carbon atom leading to their so called "recharging" within the conjugated chain. The observed large differences in the fluorescence quantum yields and lifetimes from toluene to ACN are probably connected with the large reorganization of the solvent shells in the polar solvent ACN in the excited state.

For the dye G188 with the longest conjugated chain, we suppose that the ground state represents a mixture of a "polymethine-like" structure, connected with the donor–acceptor properties of the terminal groups, and a "polyene-like" structure, mainly determined by a polyenic-type of conjugated chain with strong BLA. The relative contribution of these two resonance structures to the ground state is controlled by the polarity of the solvent: a more polar solvent can increase the ground-state polarization and make the charge-separated form dominant. The neutral polyenic form dominates in less polar toluene resulting in a change of the absorption shape (growth of the short wavelength shoulder), clearly seen in Fig. 1c. Dye G40 presumably represents an intermediate case between the shortest G19 and the longest G188 based on linear absorption data and quantum-chemical analysis. Analyzing the shift of the absorption peaks with the lengthening of the chromophore, we note that an increase in the conjugation length from G19 to G188, leads to a shift of $\approx$100 nm in ACN and $\approx$70 nm in toluene, which is in accord with the presented model of a co-existence of "polyenic-like" and "polymethine-like" forms.

It is necessary to note that quantum-chemical calculations, typically performed for the isolated molecules (in the "gas phase"), are not able to accurately reproduce the experimental data for donor–acceptor compounds, which are sensitive to the solvent polarity. Therefore, for each dye, we performed calculations for two resonance forms with the equalized bond lengths (based on X-ray measurements and referred to below as X-ray geometry) and alternated bond lengths (based on AM1 optimal geometry and referred to below as the BLA geometry) separately. The procedure of geometry optimization was stopped when the energy gradient reached 0.01 kcal/mol. The energies of the molecular orbitals (MOs), electronic transitions between them, and oscillator strengths were calculated in the framework of the standard semi-empirical AM1 method (HyperChem Package). The wave functions of the excited states were built with the single configuration interaction technique taking into account 6 occupied and 3 unoccupied MOs (a total of 18 configurations). We have additionally verified that this number of configurations is sufficient to model the one- and two-photon absorption properties of the molecules studied in the near UV, visible, and near IR ranges that are covered by the experimentally measured spectra. A more detailed description of our quantum-chemical approach can be found in Ref. 34.

Our calculations show that for G19, the difference in the positions of electronic transitions for both calculated geometries (X-ray and BLA geometries) is small and does not exceed 5–7 nm; however, these geometries affect the charge distribution within the HOMO and LUMO levels, determining the character of the $S_0 \rightarrow S_1$ absorption band. For the BLA geometry, this electron transition corresponds to charge transfer from the donor to acceptor part of the molecule. For the X-ray geometry, the charge distribution at the HOMO and LUMO levels, presented in Fig. 8, is similar to the charge distribution for the symmetrical cyanine dyes studied by us previously.[6,23] At the $S_0 \rightarrow S_1$ transition, charge is transferred to the neighboring carbon atom within the conjugated chain. Comparison of the calculated electronic transitions for both geometries with the experimental absorption and anisotropy data allowed us to conclude that a better correspondence is achieved for the "polymethine-like" structure in agreement with the previous considerations. Calculations show a large energy difference ($\approx$160 nm or $\approx$6400 cm^{-1}) and a large angle ($\approx$60°) between the $S_0 \rightarrow S_1$ and $S_0 \rightarrow S_2$ transitions.

For the longer dye G40, the difference in the calculated positions of electronic transitions, depending on the geometry choice, is much larger (up to 60 nm), however, experimental data still correspond better to the same "polymethine-like" structure, especially in polar ACN. Calculations also show a large energy difference ($\approx$220 nm or $\approx$7100 cm^{-1}) and a large angle ($\approx$55°) between the $S_0 \rightarrow S_1$ and $S_0 \rightarrow S_2$ transitions. Quite different is the situation for the longest dye G188. The calculated positions of the electronic transitions based on the BLA geometry are in

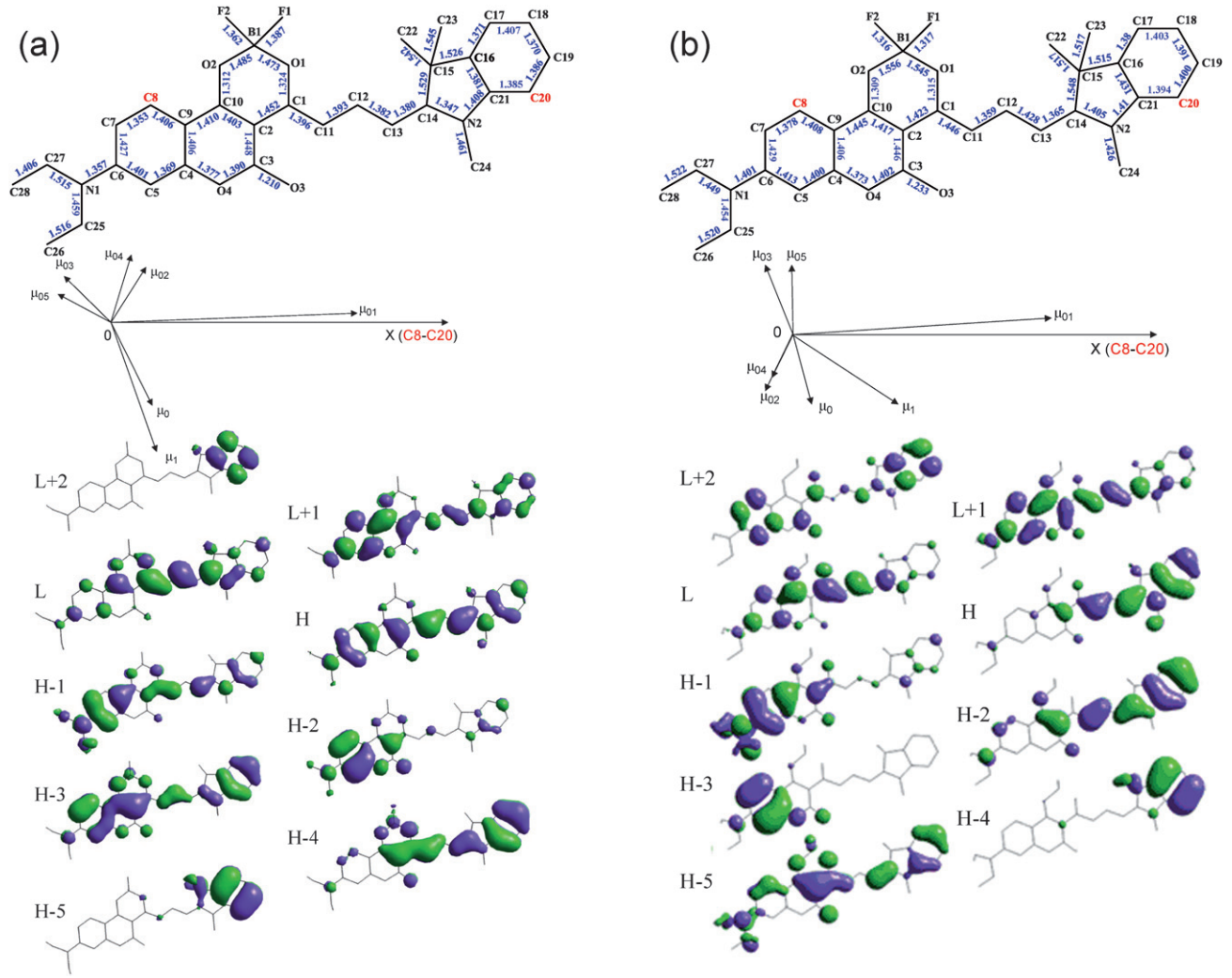

Fig. 8 Molecular geometries for G19 obtained from X-ray measurements (a) and AM1 quantum chemical calculations (b), and related orientation of transitions, state dipole moments, and molecular orbitals.

good agreement with the experimental data in the less polar solvent toluene. At the same time, calculation of the $S_0 \rightarrow S_2$ transition, based on an equalized geometry, shows $\approx$100 nm shift to the short wavelength range as compared to the anisotropy data (first decrease) obtained in the viscous solvent pTHF ($\Delta f = 0.19$). Therefore, we can conclude that the ground state in polar ACN is presented mainly by a "polymethine-like" structure, while a neutral polyenic form dominates in the less polar solvent toluene.

ESA spectra for all the asymmetrical molecules represent broad, structureless bands in the near IR region (750–1100 nm for G19; 850–1100 nm for G40, and 950–1100 nm for G188) and more intense transitions in the visible range (400–550 nm for G19; 400–600 nm for G40, and 450–650 nm for G188) as shown in Fig. 4. Due to limitations in the detector sensitivity in the infrared region, we could not accurately measure ESA longer than 1100 nm. We observe that the lengthening of the conjugation chain leads to a red shift of the ESA peaks (from 500 nm in G19 to 525 nm in G40 and 550 nm in G188); however, this red shift is much smaller than for the linear absorption peaks. Another important feature is that an increase of the conjugation length from G19 to G188 leads to an enhancement of the ESA cross-section and of the ratio between the ESA and linear absorption oscillator strengths by approximately a factor of two. These features have already been observed for the different D–π–D and D–π–A–π–D structures.[35] Our attempts to perform quantum-chemical calculations for ESA spectra in order to link them to the transitions between particular molecular orbitals, similar to previous results for symmetrical cyanines,[6,25] do not produce physically realistic results. This is partially caused by the larger change in the excited-state geometry due to the asymmetrical structure and solvatochromic effects and more mixing of the excited-state transitions involving a larger number of MOs.

3.2. 2PA spectra. Description and analysis

Experimental 1PA and degenerate 2PA spectra for G19, G40, and G188 in ACN and toluene are presented in Figs. 5–7. For comparison of transition wavelengths, these spectra are shown on the same graph with separate axes for 1PA (bottom) and 2PA (top) wavelengths. As shown in Fig. 5, the 2PA spectrum for G19 in both solvents presents two well-separated bands and

the edge of a third 2PA band. It is important to point out that we do not observe a band corresponding to two-photon excitation into the peak of the $S_0 \rightarrow S_1$ transition in spite of the asymmetrical structure of G19 and the existence of permanent dipole moments in the ground and excited states. The first 2PA band occurs at an energy shifted to the "blue" range at ≈1000–1200 cm^{-1} as compared to the peak of the $S_0 \rightarrow S_1$ transition, which is typical for the symmetrical cyanine-like molecules.[5] This 2PA band, which includes 2 peaks separated by ≈1000 cm^{-1} with cross-sections δ_{2PA} ≈400–500 GM, in general can be associated with vibrational coupling and the lowest 2PA-allowed band positioned close in energy to the 1PA-allowed band as was determined previously for some cyanine-like dyes.[5,36] A detailed quantum-chemical analysis allowed us to conclude that the nature of the first 2PA band for all dyes can be attributed to the vibrational coupling between the first excited electronic state S_1 and its vibrational modes. Our calculations show that for G19, the lowest 2PA-allowed electronic state corresponds to the second observed 2PA band with the peak position ≈830–840 nm (on the 2PA scale); δ_{2PA} ≈3000 GM in toluene and ≈2400 GM in ACN. The final state for this 2PA-allowed band corresponds to the S_2 state, which is confirmed by excitation anisotropy measurements. The edge of a third 2PA band is observed by tuning the excitation wavelength closer to the 1PA band, $S_0 \rightarrow S_1$. The peak of this third 2PA band, placed by calculation at ≈700 nm (2PA scale), cannot be reached due to the influence of the linear absorption edge. In order to understand why a change in the permanent dipole moment does not lead to the appearance of 2PA at the $S_0 \rightarrow S_1$ transition, we performed quantum-chemical calculations. These calculations show that the permanent dipole moments $\boldsymbol{\mu}_0$ and $\boldsymbol{\mu}_1$ are oriented at large angles ≈70–75° to the direction of the transition dipole moment $\boldsymbol{\mu}_{01}$. Fig. 8 illustrates the relative orientation of the state $\boldsymbol{\mu}_0$ and $\boldsymbol{\mu}_1$, and several transition dipole moments $\boldsymbol{\mu}_{0i}$ to the direction of $\boldsymbol{\mu}_{01}$ calculated for the X-ray geometry for G19 ("polymethine-like" structure). Note that the transition dipole moment $\boldsymbol{\mu}_{01}$ forms a small angle ≈8° with the direction of the conjugated chromophore, oriented along carbon atoms C8–C19. It is known that the 2PA cross-section can be calculated using a simple extension of the 3-level model proposed in Ref. 37. This model includes the same initial S_0 level, same intermediate S_1 state and two final states *f*1 (which in our case corresponds to vibrational levels of S_1) and *f*2 (which in our case corresponds to the S_2 level). Assuming that dipole moments $\boldsymbol{\mu}_{1f1}$ (equivalent to $\Delta\boldsymbol{\mu}$) and $\boldsymbol{\mu}_{1f2}$ are parallel to $\boldsymbol{\mu}_{01}$, the equation for δ_{2PA} at the excitation laser frequency ν_p, can be written as follows:

$$\delta_{2PA}(E_p) = \frac{32\pi^3}{5c^2h}\frac{{E_p}^2}{(E_{01}-E_p)^2+{\Gamma_{01}}^2}\left[\frac{|\boldsymbol{\mu}_{01}|^2|\boldsymbol{\mu}_{1f1}|^2\Gamma_{0f1}}{(E_{0f1}-2E_p)^2+{\Gamma_{0f1}}^2} + \frac{|\boldsymbol{\mu}_{01}|^2|\boldsymbol{\mu}_{1f2}|^2\Gamma_{0f2}}{(E_{0f2}-2E_p)^2+{\Gamma_{0f2}}^2}\right] \quad (5)$$

where c is the speed of light; h is Planck's constant; $E_p = h\nu_p$, $E_{01} = h\nu_{01}$, $E_{0f1} = h\nu_{f1}$, and $E_{0f2} = h\nu_{f2}$ are the corresponding transition energies and Γis a damping constant. As was suggested by Cronstrand, if there is an angle θ between the transition dipole moments $\boldsymbol{\mu}_{01}$ and $\boldsymbol{\mu}_{1fi}$, an effective excited state transition dipole moment μ_{1fi}^{eff} should be used instead, which is related to μ_{1fi} by:[38]

$$\mu_{1fi}^{eff} = \mu_{1fi}\sqrt{\frac{2\cos^2(\theta)+1}{3}} \quad (6)$$

Considering the 2PA values from Eqs. (4–5), we can conclude that the existence of the large angle θ ≈70–75° between dipole moments $\Delta\boldsymbol{\mu}$ and $\boldsymbol{\mu}_{01}$ decreases the δ_{2PA} by ≈2.6 times, and this factor probably makes this band smaller than the "vibrational coupling" 2PA band. For symmetrical molecules of C_{2V} symmetry, θ = 90° corresponding to a decrease of δ_{2PA} in 3 times. Thus, the behavior of the first 2PA band for all investigated D–π–A molecules is similar to that for symmetrical dyes.

Fig. 6 represents the 2PA spectrum for G40 in two solvents, toluene (a) and ACN (b). As shown in both solvents, the 2PA spectrum is comprised of two well-separated bands. The first band corresponding to two-photon excitation from $S_0 \rightarrow S_1$ is also associated with the "vibrational coupling band" similar to G19. This band is slightly broader in toluene than in ACN which is probably related to the smaller angle between dipole moments $\Delta\boldsymbol{\mu}$ and $\boldsymbol{\mu}_{01}$ in toluene corresponding to a more "polyenic-like" molecular geometry. The second 2PA band with peak position ≈900–910 nm (2PA scale) in both solvents shows δ_{2PA} ≈5000 GM in ACN and ≈3400 GM in toluene. The larger δ_{2PA} values in ACN are probably linked with the ≈26 nm red shift of the linear absorption peak as compared to toluene and thus, with the smaller detuning energy ($E_{01} - E_p$), leads to a stronger intermediate state resonance enhancement (ISRE).[39] The final state for this 2PA-allowed band corresponds to the S_2 state as predicted by our quantum-chemical calculations and confirmed by excitation anisotropy measurements.

Similar two-band behavior is observed for the 2PA spectrum of G188 presented in Fig. 7a, b. The first 2PA band is also linked with the coupling between the first excited electronic state and its vibrational modes and is shifted in correspondence to the solvent

Table 2 Linear and nonlinear absorption parameters of G19, G40, and G188 in toluene and acetonitrile (ACN): 1PA, $\lambda^{max}{}_{Abs}$ and $\sigma_{01}{}^{max}$ are the peak ground-state absorption wavelengths and cross-sections; ESA, λ^{max} and $\sigma_{1n}{}^{max}$ are the peak excited-state absorption wavelengths and cross-sections; and 2PA, λ^{max} and δ^{max} are the peak two-photon absorption wavelengths and cross-sections, respectively

Dye (Solvent)	1PA $\lambda^{max}{}_{Abs}$ (nm)	1PA $\sigma_{01}{}^{max}$ ($\times 10^{-16}$ cm^2)	ESA λ^{max} (nm)	ESA $\sigma_{1n}{}^{max}$ ($\times 10^{-16}$ cm^2)	2PA λ^{max} (nm)	2PA δ^{max} (GM)
G19 (toluene)	572	8.7	500	2 ± 0.4	830	3100 ± 600
G19 (ACN)	583	7.4	—	—	826	2300 ± 500
G40 (toluene)	650	6.7	530	2.4 ± 0.5	900	3200 ± 600
G40 (ACN)	678	8.8	—	—	900	5000 ± 1000
G188 (toluene)	712	4.8	550	3.8 ± 0.8	960	4700 ± 900
G188 (ACN)	777	9	—	—	980	10000 ± 2000

shift of the main peak (≈65 nm red shift in ACN). The most important result is connected with the position of the second 2PA band which remains unshifted in both solvents and is positioned at ≈960–970 nm (2PA scale) in spite of the large solvatochomic shift of the linear absorption band $S_0 \rightarrow S_1$. This effect leads to a large ISRE in ACN, allowing tuning closer to resonance and results in the greater than two times difference in 2PA cross-sections: δ_{2PA} ≈10000 GM in ACN and ≈4700 GM in toluene (Table 2). The third 2PA band for both dyes, G40 and G188, cannot be observed due to the larger shift of the linear absorption than for the 2PA peak and thus the linear absorption dominates at these wavelengths.

4. Conclusion

We have described a detailed experimental investigation of the linear and nonlinear absorption properties of a new series of asymmetrical D–π–A cyanine dyes, which contain trimethylindolin donor and diethylamino-coumarin-dioxaborine acceptor terminal groups and differ by the length of the conjugated chromophore. We also performed quantum-chemical analysis that provides insights into the nature of the linear and nonlinear processes. The measurements were performed with femto- and picosecond laser pulseswidths in order to gain a consistent understanding of the intramolecular processes and to obtain unambiguous molecular parameters. This also allows a more complete comparison with modeling of the molecular dynamics. Experimental and quantum-chemical analyses allow us to make the following conclusions:

1. All the investigated asymmetrical molecules show solvatochromic behavior which is connected with the existence of permanent ground and excited-state dipole moments. The polarity of the solvent significantly affects not only the positions of absorption and fluorescence spectral peaks but also the quantum yields and lifetime values. The largest difference in lifetimes, from 300 ps in polar ACN to 2 ns in less polar toluene (by ≈8 times), is observed for G19, which is shown to be very sensitive to the solvent polarity.

2. Excitation anisotropy spectra for all molecules reveal a large alternation of maximum and minimum features (anisotropy ranges from −0.05 to 0.35), which is quite unusual for asymmetrical structures. Anisotropy minima correspond to one-photon forbidden transitions $S_0 \rightarrow S_n$ forming ≈50–60° angles with the direction of the $S_0 \rightarrow S_1$ transition dipole moment. This large alternation of anisotropy values indicates that these molecules can be characterized by one-photon allowed and symmetry-forbidden transitions similar to symmetrical dyes and, therefore, the anisotropy can suggest the positions of the final states in the 2PA spectra.

3. The main properties of the investigated compounds can be explained based on the two resonance structures model: neutral (D–π–A) and ionic (or zwitterionic) with the separated charges (D^+–π–A^-). Our understanding is that the ground state of G19 with the shortest conjugated chain can be represented by a "polymethine-like" structure with almost equalized bond lengths within the conjugated chromophore, which is confirmed by the similar shapes of the absorption bands in solvents of different polarity as well as by X-ray crystallography measurements. For G188, with the longest conjugated chain, we suppose that the ground state represents a mixture of "polymethine-like" (with almost equalized bond lengths) and "polyene-like" (with the strong BLA) structures. Their relative contribution is controlled by the polarity of the solvent: a more polar solvent ACN increases the ground-state polarization and makes the charge-separated form more dominant. The neutral polyenic form dominates in less polar toluene resulting in a change of the absorption shape represented by a growth of the short wavelength shoulder. Dye G40 presumably represents an intermediate case between the shortest G19 and the longest G188 based on linear absorption data and quantum-chemical analysis.

4. 2PA spectra for all dyes in ACN and toluene consist of two well-separated bands (for G19 we also observed the edge of a third 2PA band). The first 2PA band occurs at an energy shifted to the "blue" range by ≈1000–1200 cm^{-1} as compared to the peak of the $S_0 \rightarrow S_1$ transition, which is typical for symmetrical cyanine-like molecules. This can be attributed to the vibrational coupling between the first excited electronic state S_1 and its vibrational modes. It is important to indicate that a change in the permanent dipole moment under two-photon excitation into the linear absorption peak does not lead to the appearance of a 2PA band as is typically observed for asymmetrical molecules. From quantum-chemical calculations we found a large angle, ≈70–75°, between $\Delta\boldsymbol{\mu}$ (change in the permanent dipole moment) and $\boldsymbol{\mu}_{01}$ (transition dipole moment) that explains a decrease in δ_{2PA} (by ≈2.6 times from calculations) which probably makes this band smaller than the "vibrational coupling" 2PA band. This behavior of the first 2PA band is similar to that for symmetrical dyes of C_{2V} symmetry with the 90° angle between $\Delta\boldsymbol{\mu}$ and $\boldsymbol{\mu}_{01}$.

5. The position of the second 2PA band for these molecules remains unshifted in both solvents of different polarity, ACN and toluene, in spite of the large solvatochomic shift of the linear absorption band $S_0 \rightarrow S_1$. This effect leads to a large intermediate state resonance enhancement in ACN, allowing tuning closer to resonance, and results in a larger δ_{2PA} in this solvent. For G188 we observe more than a two times difference in 2PA cross-sections: δ_{2PA} ≈10000 GM in ACN and ≈4700 GM in toluene. The first 2PA band follows the solvatochromic shift of the linear absorption peak and exhibits a smaller difference in 2PA cross-sections: δ_{2PA} ≈1150 GM in ACN and ≈850 GM in toluene.

Acknowledgements

We gratefully acknowledge the support of the National Science Foundation ECS 0524533, the US Army Research Laboratory W911NF0420012, the U. S. Army Research Laboratory and the U. S. Army Research Office under contract/grant number 50372-CH-MUR, and the Office of Naval Research MORPH N00014-06-1-0897. We also gratefully thank Dr Kevin Belfield for providing the time-correlated single photon counting system for fluorescence lifetime measurements.

References

1 G. S. He, L. S. Tan, Q. Zheng and P. N. Prasad, *Chem. Rev.*, 2008, **108**, 1245.
2 Seth R. Marder, *Chem. Commun.*, 2006, 131.

3 M. Pawlicki, H. A. Collins, R. G. Denning and H. L. Anderson, *Angew. Chem., Int. Ed.*, 2009, **48**, 3244.
4 H. A. Collins, M. Khurana, E. H. Moriyama, A. Mariampillai, E. Dahlstedt, M. Balaz, M. K. Kuimova, M. Drobizhev, V. X. D. Yang, D. Phillips, A. Rebane, B. C. Wilson and H. L. Anderson, *Nature Phot.*, 2008, **2**, 420.
5 J. Fu, O. V. Przhonska, L. A. Padilha, D. J. Hagan, E. W. Van Stryland, M. V. Bondar, Yu. L. Slominsky and A. D. Kachkovski, *JOSA B*, 2007, **24**, 56.
6 S. Webster, J. Fu, L. A. Padilha, O. V. Przhonska, D. J. Hagan, E. W. Van Stryland, M. V. Bondar, Y. L. Slominsky and A. D. Kachkovski, *Chem. Phys.*, 2008, **348**, 143.
7 M. Charlot, N. Izard, O. Mongin, D. Riehl and M. Blanchard-Desce, *Chem. Phys. Lett.*, 2006, **417**, 297.
8 K. D. Belfield, A. R. Morales, B. S. Kang, J. M. Hales, D. J. Hagan, E. W. Van Stryland, V. M. Chapela and J. Percino, *Chem. Mat.*, 2004, **16**, 4634.
9 M. Halik, W. Wenseleers, C. Grasso, F. Stellacci, E. Zojer, S. Barlow, J.-L. Bredas, J. Perry and S. Marder, *Chem. Commun.*, 2003, 1490.
10 M. Barzoukas and M. Blanchard-Desce, *J. Chem. Phys.*, 2000, **113**, 3951–3955.
11 F. Terenziani, G. D'Avino and A. Painelli, *Chem. Phys. Chem.*, 2007, **8**, 2433.
12 V. M. Geskin and J.-L. Bredas, *Inter. J. Quantum Chem.*, 2003, **91**, 303.
13 J. O. Morley, R. M. Morley, R. Docherty and M. H. Charlton, *J. Am. Chem. Soc.*, 1997, **119**, 10192.
14 Q. Zheng, S. K. Gupta, G. S. He, L. S. Tan and P. N. Prasad, *Adv. Funct. Mater.*, 2008, **18**, 2770.
15 M. Johnsen and P. R. Ogilby, *J. Phys. Chem. A*, 2008, **112**, 7831.
16 K. Zao, L. Ferrighi, L. Frediani, C. K. Wang and Y. Luo, *J. Chem. Phys.*, 2007, **126**, 204509.
17 J. Fu, O. V. Przhonska, L. A. Padilha, D. J. Hagan, E. W. Van Stryland, M. V. Bondar, Yu. L. Slominsky and A. D. Kachkovski, *JOSA B*, 2007, **24**, 67.
18 S.-J. Chung, S. Zheng, L. Beverina, T. Odani, Jie Fu, L. A. Padilha, A. Biesso, J. M. Hales, X. Zhan, K. Schmidt, A. Ye, E. Zojer, S. Barlow, D. J. Hagan, E. W. Van Stryland, Y. Yi, Z. Shuai, G. A. Pagani, J.-L. Bredas, J. W. Perry and S. R. Marder, *J. Am. Chem. Soc.*, 2006, **128**, 14444.
19 A. O. Gerasov, M. P. Shandura and Y. P. Kovtun, *Dyes and Pigments*, 2008, **77**, 598.
20 J. R. Lakowicz, *Principles of Fluorescence Spectroscopy*, Kluwer Academic/Plenum Publishers, New York, 1999.
21 F. Wurthner, G. Archetti, R. Schmidt and H. G. Kuball, *Angew. Chem., Int. Ed.*, 2008, **47**, 4529.
22 D. Magde, J. H. Brannon, T. L. Cremers and J. Olmsted, *J. Phys. Chem.*, 1979, **83**, 696.
23 S. Webster, L. A. Padilha, H. Hu, O. V. Przhonska, D. J. Hagan, E. W. Van Stryland, M. V. Bondar, I. G. Davydenko, Y. L. Slominsky and A. D. Kachkovski, *J. Lumin.*, 2008, **128**, 1927.
24 R. A. Negres, O. V. Przhonska, D. J. Hagan, E. W. Van Stryland, M. V. Bondar, Yu. L. Slominsky and A. D. Kachkovski, *IEEE J. Quantum Electron.*, 2001, **7**, 849.
25 L. A. Padilha, S. Webster, H. H. Hu, O. V. Przhonska, D. J. Hagan, E. W. Van Stryland, M. V. Bondar, I. G. Davydenko, Y. L. Slominsky and A. D. Kachkovski, *Chem. Phys.*, 2008, **352**, 97.
26 M. Sheik-Bahae, A. A. Said, D. J. Hagan and E. W. Van Stryland, *IEEE J. Quantum Electron.*, 1990, **26**, 760.
27 R. S. Lepkowicz, O. V. Przhonska, J. M. Hales, J. Fu, D. J. Hagan, E. W. Van Stryland, M. V. Bondar, Yu. L. Slominsky and A. D. Kachkovski, *Chem. Phys.*, 2004, **305**, 259.
28 C. Xu and W. W. Webb, *JOSA B*, 1996, **13**, 481.
29 F. Meyers, S. R. Marder, B. M. Pierce and J.-L. Bredas, *J. Am. Chem. Soc.*, 1994, **116**, 10703.
30 F. Terenziani, C. Katan, E. Badaeva, S. Tretiak and M. Blanchard-Desce, *Adv. Mater.*, 2008, **20**, 4641.
31 D. J. Watkin, C. K. Prout, J. R. Carruthers, P. W. Betteridge. *CRYSTALS, Issue 10*, Oxford: Chemical Crystallography Laboratory, University of Oxford, 1996.
32 N. Tyutyulkoy, J. Fabian, A. Mehlhorn, F. Dietz, and A. Tadjer, *Polymethine Dyes. Structure and Properties*. St. Kliment Ohridski University Press, Sofia. 1991, p.328.
33 A. O. Gerasov, M. P. Shandura, Y. P. Kovtun and A. D. Kachkovsky, *J. Phys. Org. Chem.*, 2008, **21**, 419.
34 S. Dahne, *Science*, 1978, **199**, 1163.
35 R. S. Lepkowicz, C. M. Cirloganu, J. Fu, O. V. Przhonska, D. J. Hagan, E. W. Van Stryland, M. V. Bondar, Y. L. Slominsky and A. D. Kachkovski, *JOSA B*, 2005, **22**, 2664.
36 D. Scherer, R. Dorfler, A. Feldner, T. Vogtmann, M. Schwoerer, U. Lawrentz, W. Grahn and C. Lambert, *Chem. Phys.*, 2002, **279**, 179.
37 K. Kamada, K. Ohta, Y. Iwase and K. Kondo, *Chem. Phys. Lett.*, 2003, **372**, 386.
38 Peter Cronstrand, Yi Luo and Hans Agren, *Chem. Phys. Lett.*, 2002, **352**, 262.
39 J. M. Hales, D. J. Hagan, E. W. Van Stryland, K. J. Schafer, A. R. Morales, K. D. Belfield, P. Pacher, O. Kwon, E. Zojer and J. L. Bredas, *J. Chem. Phys.*, 2004, **121**, 3152.